Supporting Information

for

Facile and Visualizable Identification of Broad-Spectrum Inhibitors of MDM2/p53 Using Co-expressed Protein Complexes

Experimental Details

Plasmid construction

The co-expressed plasmid containing genes encoding His_6-MDM2 and p53-GSG-GFP/mCherry was constructed by three-step PCR. Firstly, the gene encoding MDM2 (aa 17-125) and his_6-tag was amplified from MDM2-PGEX-4T-1 plasmid by polymerase chain reactions (PCR) with the following primers: 5'-GGAATTCcatatgCACCATCATCATCATCACTCACAGATTCC-3' (forward, NdeI site denoted in lower-case letters and his_6-tag underlined), and 5'-CGgaattcCTAGTTCTCACTCACAGATGTACC-3' (reverse, EcoRI site denoted in lower-case letters and a stop codon underlined). The PCR product was cloned into the NdeI and EcoRI sites of a modified vector derived from bacterial expression vector pET21b with an N-terminal his_6-tag (Novagen). Secondly, the gene encoding GFP (aa 1-236) and a second ribosome binding site (RBS) were amplified from sfGFP-pBAD plasmid using oligonucleotide the following primes: 5'-CGgaattcAAATAATTTTGTTTAACTTTAAGAAGGAGATGTC-3' (forward, containing an EcoRI site denoted in lower-case letters and RBS underlined) and 5'-CATGccatggTCCTGATCCGAGTTCGTCCA-3' (reverse, containing an NcoI site denoted in lower-case letters and GSG linker underlined). The gene was cloned into the EcoRI site and NcoI site of same vector. Finally, the gene encoding p53 (aa 15-29) was added using the following primes: 5'-CATGccatggAGTCAGGAAACATTTTCAGACCTA-3' (forward, containing an NcoI site denoted in lower-case letters) and 5'-CCGctcgagCTAGTTTTCAGGAAGTAGTTTCCATAG-3' (reverse, containing an XhoI site denoted in lower-case letters and a stop codon denoted). The genes were cloned into the same NcoI site and NcoI site of pET21b vector.

For constructing the fusion protein containing mCherry, the same procedure was conducted by using the gene encoding mCherry (aa 1-236) instead of GFP. mCherry and a second ribosome binding site (RBS) were amplified from mCherry-pBAD using oligonucleotide primes 5'-GCgaattcAAATAATTTTGTTTAACTTTAAGAAGGAGATGTTG-3' (forward, containing an EcoRI site denoted in lower-case letters and RBS underlined) and 5'- CATGccatggTCCTGATCCCTTGTACAG-3' (reverse, containing an NcoI site denoted in lower-case letters and GSG linker underlined). All constructs were confirmed by PCR-based sequencing. These constructs are named MDM2/p53-GFP pET-21b and MDM2/p53-GFP pET-21b (Figure S1).

Preparation and characterization of platinum complexes

cis-$[Pt(NH_3)_2(Xan)_2]_2(NO_3)_2$: Cisplatin was dissolved in DMF and 1.98 equivalents of $AgNO_3$ were added. The reaction stirred overnight (16 h) in darkness at room temperature and was then filtered through celite to remove precipitated AgCl. The solution was then moved to darkness and 2.01 equivalents of xanthosine dihydrate were added and the reaction continued at room temperature for 72 hours. The solution was then brought to dryness and 5 mL of H_2O was added. Insoluble material was filtered off and the resulting colorless filtrate was reduced to ~1 mL and excess acetone was added to precipitate out a white solid. The product may be recrystallized from H_2O/acetone. Anal. Calc. for $C_{20}H_{30}N_{12}O_{18}Pt.2H_2O$: C: 25.08, H: 3.55, N: 17.55. Found; C: 25.16 H: 3.33 N: 16.85. δ(^{1}H) NMR (D_2O): 3.88 (4H, t), 4.31 (2H, q), 4.34 (2H, t), 4.42 (2H, br s) 4.49 (2H, t), 5.88 (2H, d), 8.38 (2H, s). δ(^{195}Pt) NMR: -2417.33 ppm.

cis-$[Pt(NH_3)_2(Guo)_2]_2(NO_3)_2$: This was synthesized in a similar manner to the xanthosine derivative. Cisplatin was dissolved in DMF and 1.98 equivalents of $AgNO_3$ were added. The reaction stirred overnight (16 h) in darkness at room temperature and was then filtered through celite to remove precipitated AgCl. The solution was then moved to darkness and 2.01 equivalents of guanosine were added and the reaction continued at room temperature for 72 hours. The solution was then brought to dryness and 5 mL of H_2O was added. Insoluble material was filtered off and the resulting colorless filtrate was reduced to ~1 mL and excess acetone was added to precipitate out a white solid. The product may be recrystallized from H_2O/acetone. Anal. Calc. for $C_{20}H_{32}N_{14}O_{16}Pt{\cdot}2H_2O$; C: 25.13, H: 3.77, N: 20.52. Found; C: 24.59, H: 3.39, N: 20.20. δ(^{1}H) NMR (D_2O): 3.84 (4H, dd), 4.21 (2H, q), 4.31 (2H, t), 4.40 (2H, br s), 4.61 (2H, t), 5.90 (2H, d), 8.38 (2H, s). δ (^{195}Pt) NMR: -2424.82 ppm

Inhibition assay

For the fluorescent titration, 200 µl Ni-NTA was transferred into a spin column, the excess buffer (20 mM Tris, pH 8.0, 200 mM NaCl) was removed by centrifugation. The protein complex (MDM2/p53-GFP or MDM2/p53-mCherry) was prepared in 20 µM in 20 mM Tris buffer (pH 8.0, containing 200 mM NaCl). 400 µl protein complex was incubated with Ni-NTA in the spin column for 5 min with shaking. Then the inhibitor was added to the spin column with Ni-NTA gradually. The mixture was incubated for another 5 min to reach the equilibration of inhibitor binding. Then the supernatant was collected by centrifugation at the bottom of the spin column by centrifugation, and the fluorescence of supernatant was measured.

Calculation of inhibitory constants

The binding affinity of inhibitors to MDM2 was obtained by titration of inhibitors to the MDM2/p53-GFP protein complex, by which the fluorescent protein p53-GFP was released from the resin. The volume increasement during titration (from 400 µl to 414 µl at the end of titration) was calibrated for the fluorescence intensity measurement. The apparent dissociation constants of inhibitors to MDM2 were determined by fitting fluorescence change during the titration using the following bimolecular association model according to the literature.

$$PA+B \underset{}{\overset{K}{\rightleftharpoons}} PB+A$$

$$\mathbf{K} = \frac{\mathbf{K_B}}{\mathbf{K_A}} = \frac{[\mathbf{B}] - [\mathbf{PA}]}{[\mathbf{A}] - [\mathbf{PB}]} = \frac{([\mathbf{B}]_\mathbf{0} - [\mathbf{PB}])([\mathbf{A}]_\mathbf{0} - [\mathbf{A}])}{[\mathbf{A}] - [\mathbf{PB}]}$$

$$[\mathbf{PB}] = [\mathbf{P}]_\mathbf{0} - \frac{(\mathbf{K_A} + [\mathbf{A}])([\mathbf{A}]_\mathbf{0} - [\mathbf{A}])}{[\mathbf{A}]}$$

Where P, A and B denote MDM2, p53 and inhibitor, respectively. K_A and K_B are dissociation constants of MDM2 to p53 and inhibitors, respectively. $[P]_0$, $[A]_0$ and $[B]_o$ are the concentrations of total of protein, A and B, respectively. The data fitting was performed using Origin 2017. The mean values of K_B were determined from three independent measurements.

Surface plasmon resonance (SPR) analysis

SPR analyses were performed on a Biacore T200 (GE Healthcare). CM5 chips were preconditioned using short pulses (2 µl/s × 50 s) of 50 mM NaOH with 0.5% (v/v) SDS and 50 mM NaOH. All experiments were performed at 25 °C in 50 mM phosphate buffer containing 50 mM NaCl at pH 6.8. The MDM2 protein was immobilized on a CM5 sensor chips. The measurements were performed with resonance units at a flow rate of 30 µl/s.

NMR spectroscopy

NMR spectra were recorded on a Bruker 600M Hz spectrometers equipped with cryogenic probes. 0.4 mM ^{15}N labeled protein samples were prepared in 50 mM sodium phosphate buffer (containing 50 mM NaCl, 5 mM DTT and 10% D_2O) at pH 6.8. ^{1}H-^{15}N HSQC spectra were recorded at 25°C in states-

TPPI mode for quadrature detection. Data were processed using NMR Draw and Sparky. The peak assignment was performed using the assignment by Stoll et al.[1]

Molecular dynamics simulations

Starting from the initial protein-ligand complex structure model obtained from COACH-D method, a 100 ns MD simulation was performed with a parallel implementation of the GROMACS-5.0.4 package. Amber14SB force field was used for the protein. For the ligand, the force field parameters were taken from the general AMBER force field (GAFF)[2] and the partial charges were computed using the am1-bcc[3] method. The periodic boundary condition (PBC) with a cubic box type was used, with the minimal distance of 1.2 nm between the solute and the box boundary. TIP3P[4] water molecules were added into the box. The steepest descent method was used for the energy-minimization of the system until the maximum force on any atom was less than 1000 kJ/(mol·nm). To neutralize the net negative charge of the system and to mimic the physiological salt concentration value of 150 mM, 27 Na ions and 32 Cl ions were added to the system by replacing water molecules with the most favorable electrostatic potential. The final system was energy minimized using the steepest descent followed by the conjugate gradient method until the maximum force on any atom was less than 100 kJ/(mol·nm). Verlet integration scheme[5] was used with a 2 fs time-step. A 100 ps equilibration simulation with positional restraint was firstly performed, using a force constant of 1000 kJ mol^{-1} nm^{-2}. The initial atomic velocities were generated according to a Maxwell distribution at 310 K. The following production run was 100 ns long. The simulation was performed in a constant NPT ensemble, and the system was coupled to a temperature bath of 310 K through use of a velocity rescaling thermostat.[6] The pressure was adjusted to 1 bar with a relaxation time of 2.0 ps, and the compressibility was 4.5×10^{-5} bar^{-1} by the Parrinello-Rahman pressure coupling method.[7] Covalent bonds were constrained using the LINCS algorithm.[8] The cutoff distances for the Coulomb and van der Waals interactions were chosen to be 0.9 and 1.4 nm, respectively, and the neighbor list was updated every 10 fs. The long-range electrostatic interactions were treated by the PME algorithm,[9] with a tolerance of 10^{-5} and an interpolation order of 4.

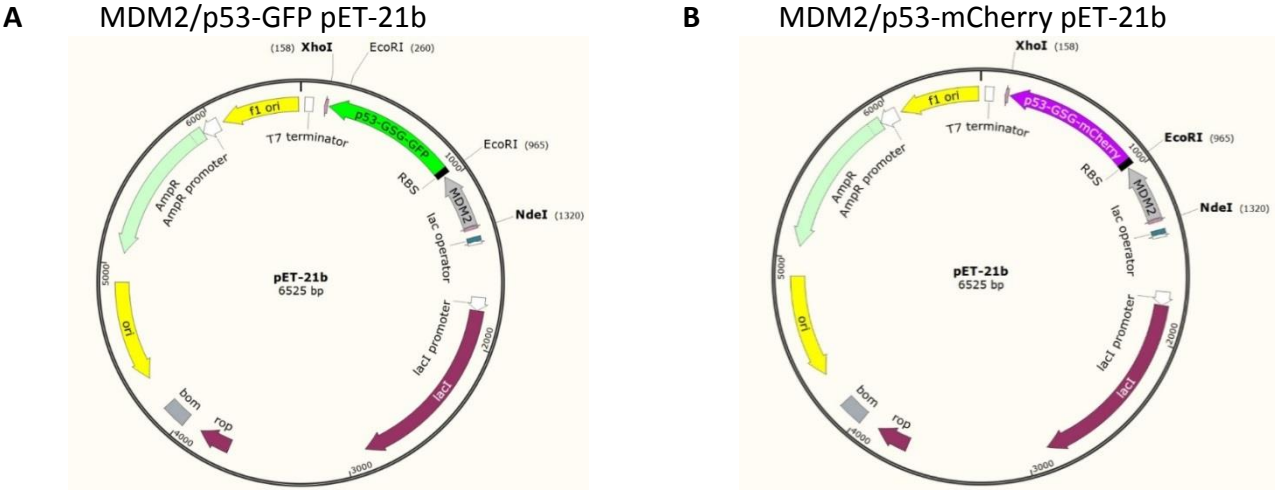

Figure S1. The co-expressed plasmid maps. (A) MDM2/p53-GFP pET-21b; (B) MDM2/p53-mCherry pET-21b.

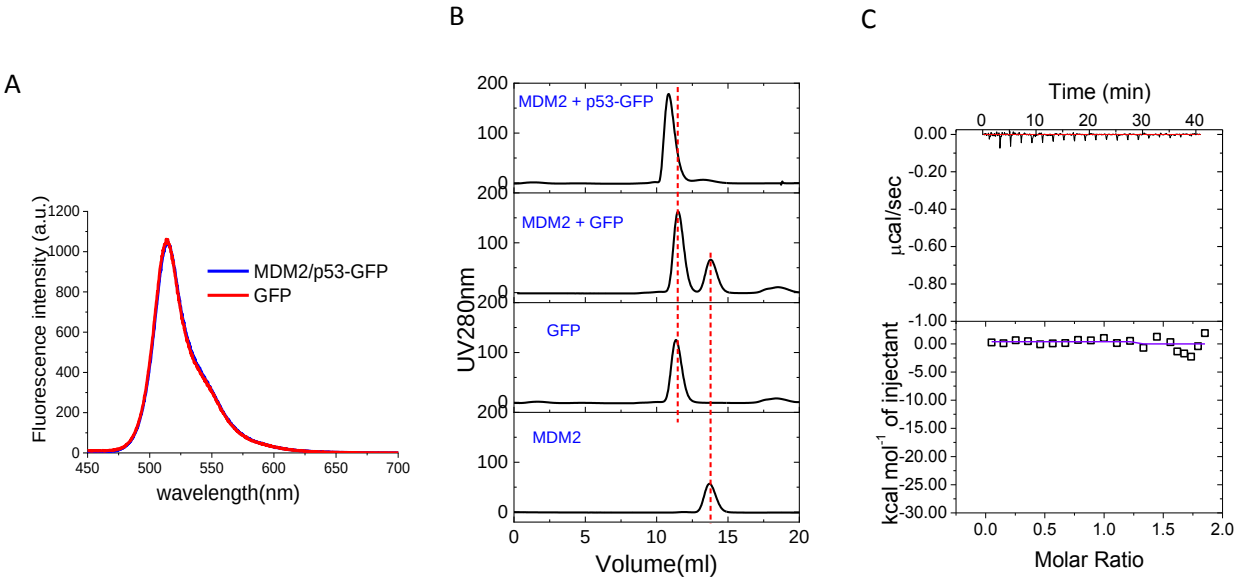

Figure S2. The influence of the fusion of p53-GFP on the function of individual protein domains. (A) The fluorescence spectra of MDM2/p53-GFP and GFP protein. The spectra were recorded in 80 µM protein with excitation wavelength 420 nm. (B) Gel filtration analyses of MDM2 protein, GFP protein, and the interaction between MDM2 and GFP. For measuring the protein interaction, MDM2 was incubated with GFP or p53-GFP for 2 h at room temperature in 20 mM Tris solution (pH 8.0). (C) ITC measurement of MDM2 with GFP protein. 400 µM MDM2 in the syringe was titrated into 40 µM GFP in cell.

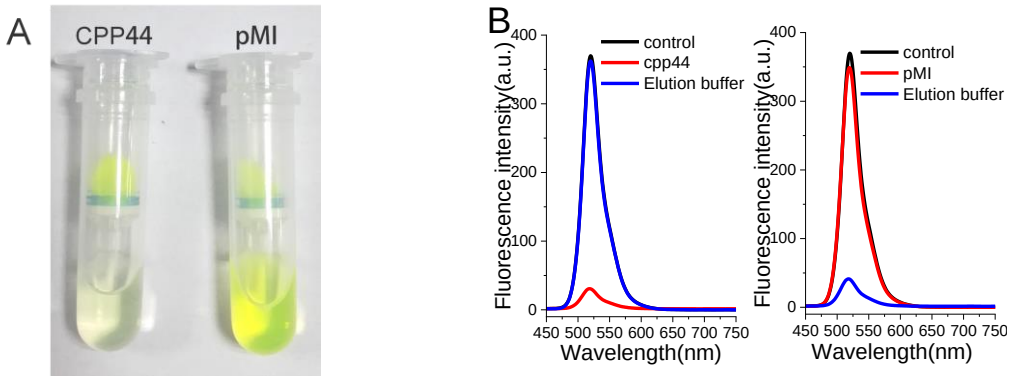

Figure S3. The comparison of the inhibitory effect of CPP44 and pMI on the MDM2/p53-GFP interaction. (A) Visualization of the inhibitory effect using MDM2/p53-GFP loaded Ni-NTA resin. 10 µM CPP44 or pMI was added to the resin in the spin column. (B) Fluorescence spectra of samples from the spin column after adding 100 µM ligands (CPP44 or pMI). The colors denote the solution in the spin column after adding ligands (red), and the remaining proteins eluted from Ni-NTA resin (blue). The control spectra (black) were recorded on the MDM2/P53-GFP complex before loading to the resin. 10 µM MDM2/p53-GFP protein was used in the measurement and the excitation wavelength of fluorescence is 420 nm.

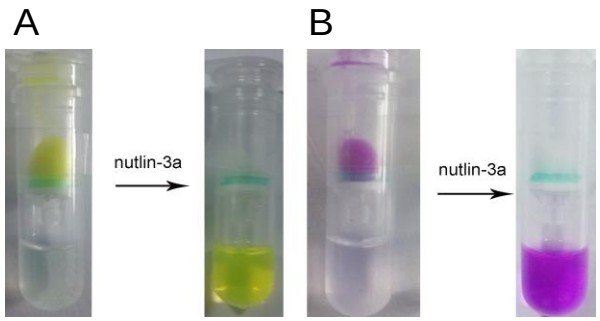

Figure S4. Visualization of nutlin-3a inhibition of MDM2/p53 interaction on the protein complex loaded Ni-NTA resin. (A) MDM2/p53-GFP; (B) MDM2/p53-mCherry. 400 µl protein complexes (40 µM) in 20 mM Tris buffer (pH 8.0, 200 mM NaCl) were loaded to the resin and 400 µM nutlin-3a was added.

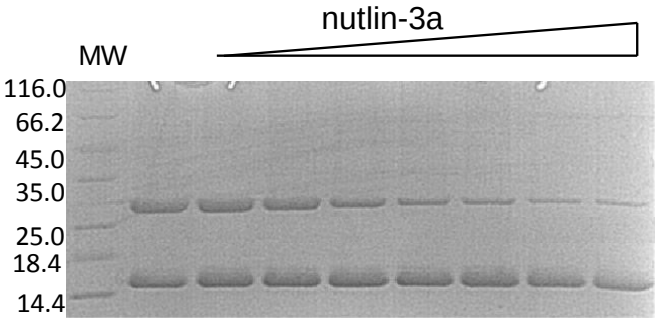

Figure S5. Detection of inhibition effect of nutlin-3a on the interaction of MDM2/p53-GFP complex using 15% Tris-Tricine SDS-PAGE. 400 µl 100 µM protein complex in 20 mM Tris buffer (pH 8.0, 200 mM NaCl) was loaded to Ni-NTA resin and increasing amount of nutlin-3a (0 - 400 µM from left to right) was added. After removal of supernatant, the protein remained in resin was analyzed.

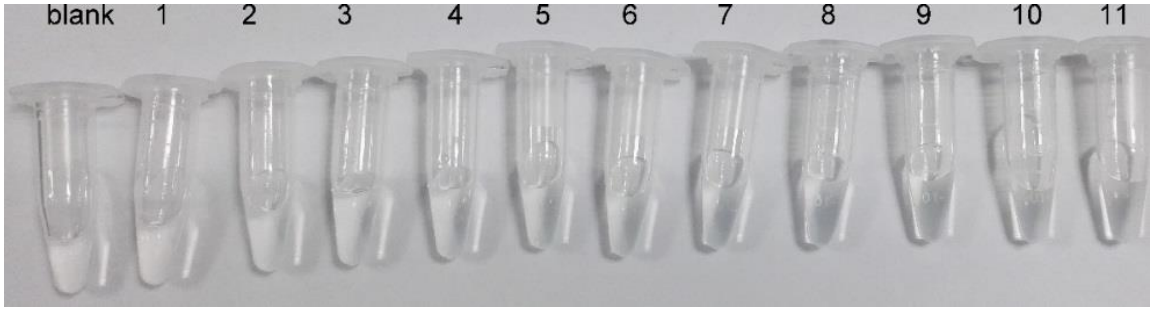

Figure S6. Test the inhibition of p53/MDM2 interaction using a series of pyrrolidine derivatives and aromatic compounds. 400 µl 10 µM MDM2/p53-GFP fusion protein in 20 mM Tris buffer (pH 8.0, 200 mM NaCl) was loaded in Ni-NTA in 20 mM Tris-HCl buffer (pH 8.0), 200 mM NaCl. After incubation with various small molecules for 5 min, the flow through from spin column was collected. DMSO was used as control.

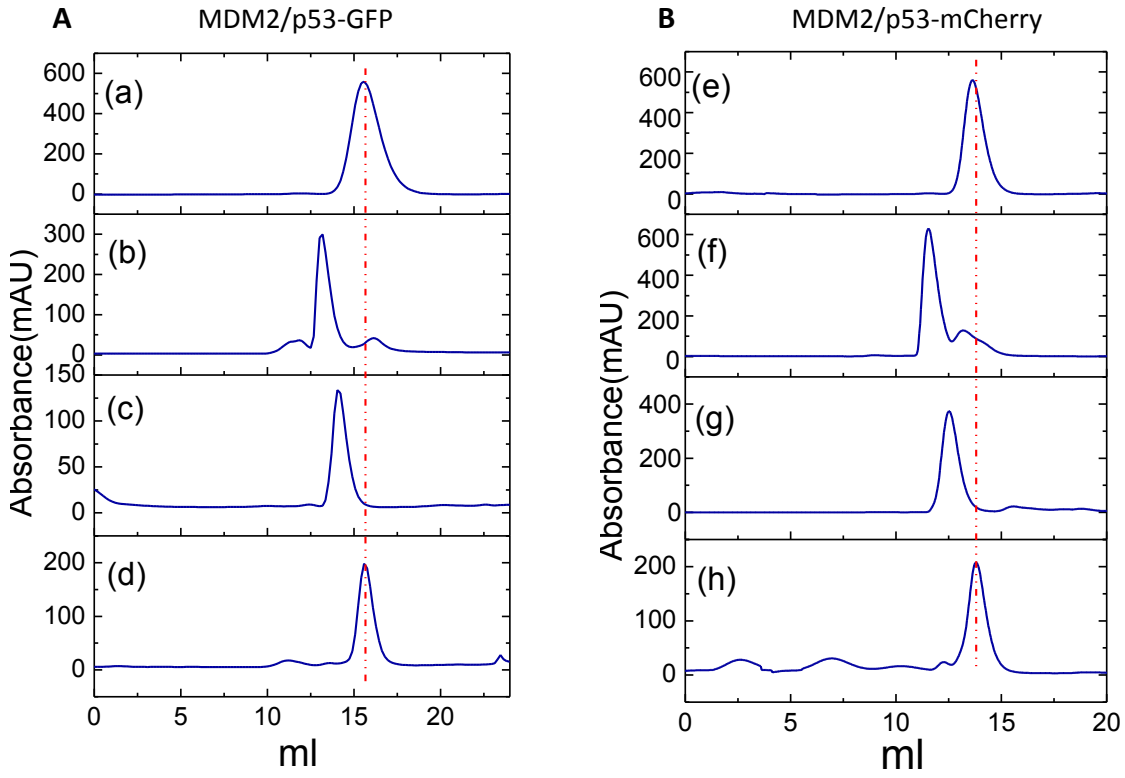

Figure S7. Gel filtration analysis of MDM2/p53-GFP (A) and MDM2/p53-mCherry (B). (a, e) purified MDM2 protein; (b, f) protein complexes of MDM2/p53-GFP or MDM2/p53-mCherry eluted from Ni-NTA column using elution buffer (20 mM Tris, pH 8.0,200 mM NaCl, 250 mM imidazole); (c, g) the supernatant of MDM2/p53-GFP or MDM2/p53-mCherry loaded Ni-NTA resin after the incubation with pMI from Ni-NTA; (d, h) proteins remaining in Ni-NTA resin from (c, g) was eluted by elution buffer.

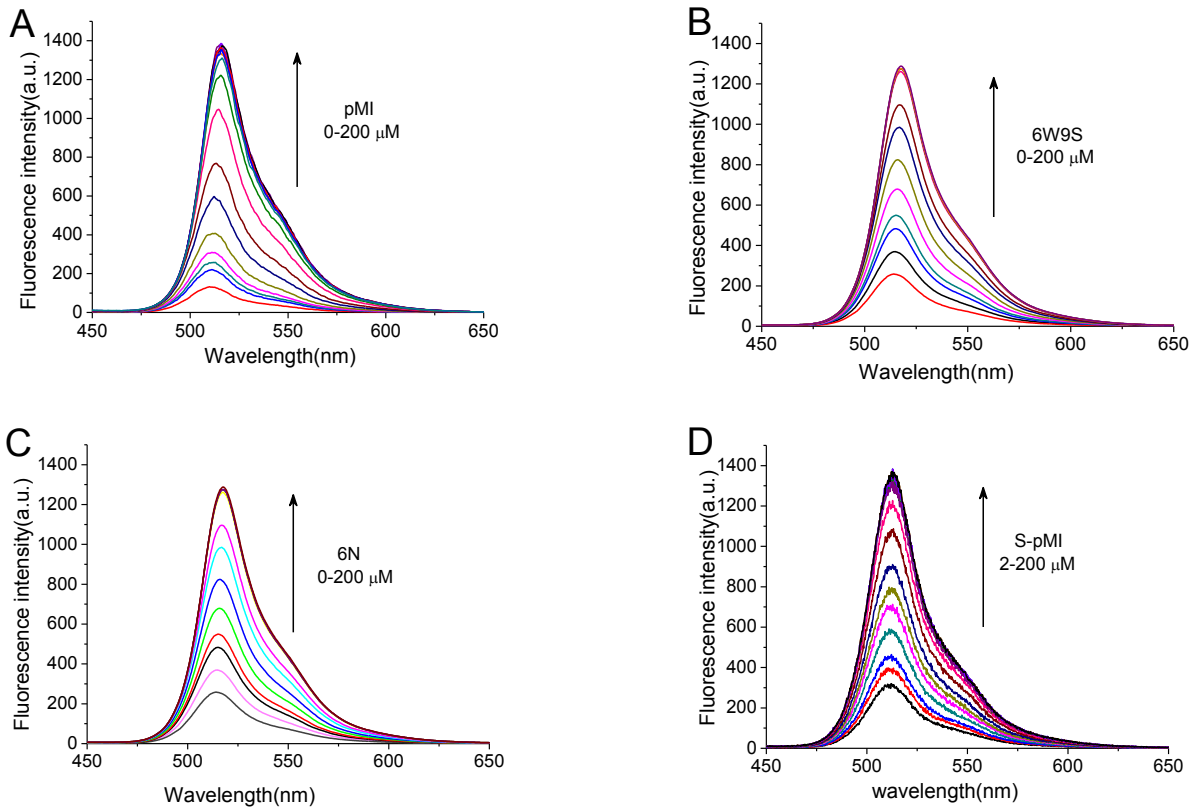

Figure S8. Fluorescent titration of peptide to the protein complex MDM2/p53-GFP. (A) pMI; (B) 6W9S; (C) 6N; (D) S-pMI. 20 μM MDM2/p53-GFP (400 μl) was loaded in Ni-NTA. The fluorescence of supernatant was measured upon adding inhibitors from 2 to 200 μM.

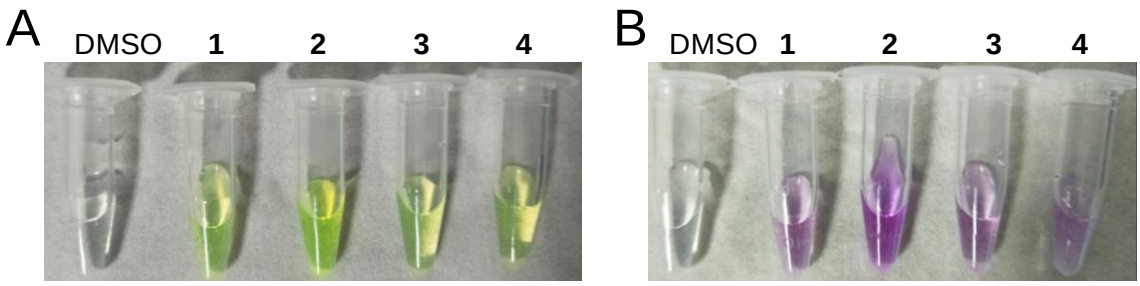

Figure S9. Test the inhibition of p53/MDM2 interaction using four cyclohexyl-triphenylamine derivatives**.** 400 μl 10 μM MDM2/p53-GFP (A) and MDM2/p53-mCherry (B) fusion protein in 20 mM Tris buffer (pH 8.0, 200 mM NaCl) was loaded in Ni-NTA in 20 mM Tris-HCl buffer (pH 8.0), 200 mM NaCl. After incubation with equivalent cyclohexyl-triphenylamine compounds for 5 min, the flow through from spin column was collected. DMSO was used as control.

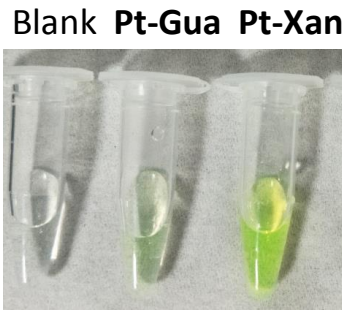

Figure S10. Test the inhibition of p53/MDM2 interaction using two platinum-nucleoside complexes**.** 400 µl 10 µM MDM2/p53-GFP fusion protein in 20 mM Tris buffer (pH 8.0, 200 mM NaCl) was loaded in Ni-NTA in 20 mM Tris-HCl buffer (pH 8.0), 200 mM NaCl. After incubation with equivalent Pt complexes for 5 min, the flow through from spin column was collected. Tris buffer was used as control.

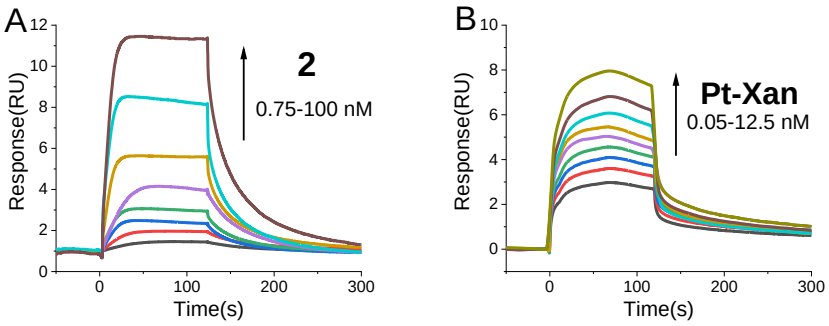

Figure S11. Binding kinetics of inhibitors to MDM2 (aa 17-125) measured by SPR spectroscopy. (A) cyclohexyl-triphenylamine **2**; (B) (*cis*-[Pt(NH_3)$_2$(xanthosine)$_2$](NO_3)$_2$) (**Pt-Xan**). MDM2 was immobilized on chips. The data were calculated from three separate measurements.

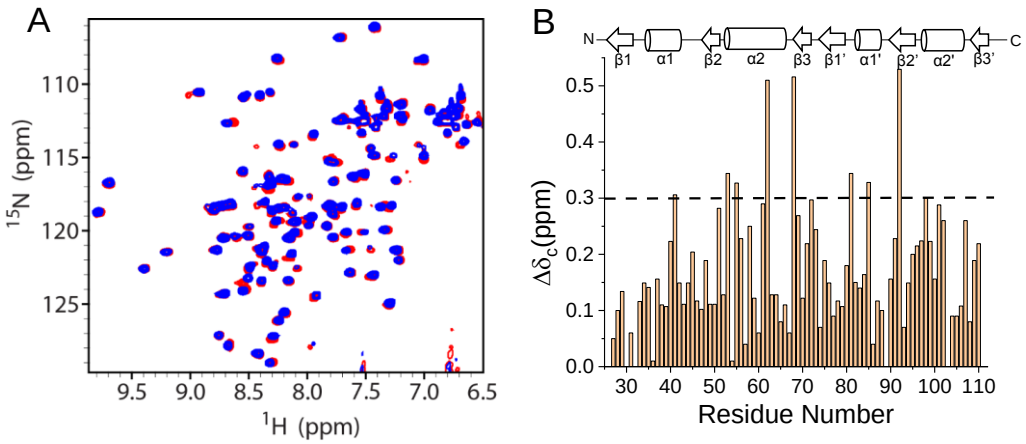

Figure S12. NMR chemical shift perturbation measurement. (A) Overlaid 2D ^{1}H-^{15}N HSQC spectra for ^{15}N-labeled MDM2 in the absence (red) or in the presence (blue) of the **2**. The NMR spectra were collected in sodium phosphate buffer and 0.2 molar ratio of **2** was added to MDM2. (B) Chemical shift perturbation of MDM2 in the NMR spectra. The chemical shift changes were calculated using $\Delta\delta_C = \sqrt{(5\delta_H)^2 + (\delta_N)^2}$ according to literature.[10]

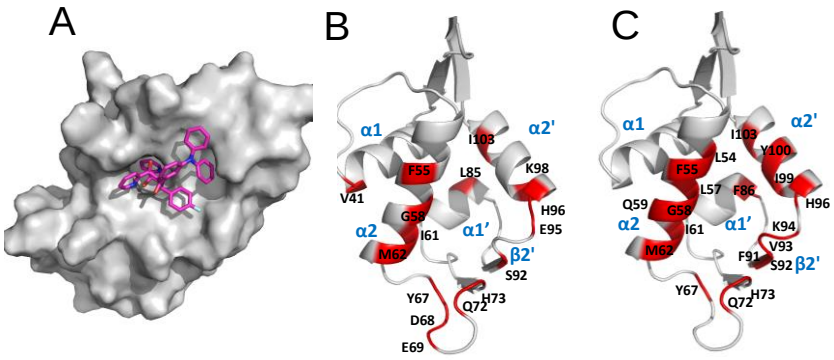

Figure S13. Structure simulation of MDM2/**2** complex. (A) The final structure from MD simulation. MDM2 is shown in gray surface and **2** is shown in sticks. (B) Secondary structure of MDM2, in which the red color indicates residues exhibit obvious chemical shift change on NMR spectra upon the binding of **2**. (C) Secondary structure of MDM2, in which the red color indicates residues interact with **2** in the structure.

Table 1. Dissociation constants[a] (nM) to MDM2 measured from fluorescence titration.

Inhibitors	Nutlin-3a	pMI	S-pMI	6N	6W9S
K_d	25±1	4.8±1.8	77±8	73.2±4.6	16.2±1.7

[a] Based on the dissociation constant of p53 (K_d = 600 nM).[11]

References

1. R. Stoll, C. Renner, P. Muhlhahn, S. Hansen, R. Schumacher, F. Hesse, B. Kaluza, R. A. Engh, W. Voelter and T. A. Holak, *J. Biomol. NMR*, 2000, **17**, 91-92.
2. J. M. Wang, R. M. Wolf, J. W. Caldwell, P. A. Kollman and D. A. Case, *J. Comput. Chem.*, 2004, **25**, 1157-1174.
3. A. Jakalian, D. B. Jack and C. I. Bayly, *J. Comput. Chem.*, 2002, **23**, 1623-1641.
4. W. L. Jorgensen, J. Chandrasekhar, J. D. Madura, R. W. Impey and M. L. Klein, *J. Chem. Phys.*, 1983, **79**, 926-935.
5. L. Verlet, *Phys. Rev 1967, **159**, 98-103*.
6. G. Bussi, D. Donadio and M. Parrinello, *J. Chem. Phys.*, 2007, **126**.
7. M. Parrinello and A. Rahman, *J. Appl. Phys.*, 1981, **52**, 7182-7190.
8. B. Hess, *J. Chem. Theory Comput.*, 2008, **4**, 116-122.
9. U. Essmann, L. Perera, M. L. Berkowitz, T. Darden, H. Lee and L. G. Pedersen, *J. Chem. Phys.*, 1995, **103**, 8577-8593.
10. S. W. Chi, S. H. Lee, D. H. Kim, M. J. Ahn, J. S. Kim, J. Y. Woo, T. Torizawa, M. Kainosho and K. H. Han, *J. Biol. Chem.*, 2005, **280**, 38795-38802.
11. P. H. Kussie, S. Gorina, V. Marechal, B. Elenbaas, J. Moreau, A. J. Levine and N. P. Pavletich, *Science*, 1996, **274**, 948-953.